PAPER

Check for updates

Detection of nitrous oxide using infrared optical plasmonics coupled with carbon nanotubes†

Thomas Allsop, [ID] *[abc] Mohammed Al Araimi,[de] Ron Neal,[f] Changle Wang,[b] Phil Culverhouse,[f] Juan D. Ania-Castañón,[a] David J. Webb,[b] Paul Davey,[f] James M. Gilbert[c] and Alex Rozhin[bd]

Interest in gas sensing using functionalised carbon nanotubes is a major area of research that utilises changes in their electrical properties induced by the reaction with a specific gas. This paper describes specific gas sensing on an optical platform consisting of a 2-dimensional nano-structured plasmonic array of nano-antennae/nanowires, with topological dimensions of mean radius of 130 nm, typical length of 20 μm and a period of 500 nm. The array is created by the spatial compaction of germanium oxides when the material interacts with ultra-violet irradiance, it can support infra-red localised surface plasmons. Carbon nanotubes are deposited upon the surface of the plasmonic platform followed by the application of the polyethyleneimine polymer. The resulting nanomaterials-photonic platform gives rise to the selective response to nitrous oxide gases, which are a major contributor to atmospheric degradation. We achieve the device sensitivity up to 100% atmosphere of nitrous oxide with a detection limit of 109 ppm, a maxiumum response time of nineteen seconds and yielding a full-scale deflection of +5.7 nm. This work demonstrates that the optical properties of specific carbon nanotubes can be used in a wide range of sensing applications offering a new sensing paradigm.

1. Introduction

Functionalised carbon nanotubes (FCNs) have been a subject of intense research over the last couple of decades with various applications in the field of analytical chemistry, such as, chemical separation, extraction (such as the removal of heavy metals from water), as well as chromatographic analysis, along with uses in the fields of electrochemistry and medicine.[1–4] There is another major area of application for FCNs in the field of sensing, with particular emphasis on gas sensing, with a number of publications[5–7] dealing with specific gas detection. This interest has grown from an awareness of the shortcomings in conventional gas sensing[8] and those of more recent developments using metal-oxide semiconductors (MOS).[9,10] MOS detection schemes have been shown to have advantages over

more conventional spectroscopic techniques that rely on the measurement of absorption features,[11] such as lower fabrication costs, miniaturisation, integration and multiplexing capabilities. On the other hand, the weakness of MOS sensing schemes are issues related to stability and chemical selectivity along with their need to operate above ambient temperature. In addition, there is the problem of spark hazards because of their electrical operation, which is a significant problem in the detection of methane and other potentially explosive gases.[10,11] FCNs based sensors have demonstrated a good chemical selectivity, stability and regeneration. The vast majority of the detection protocols of FCNs sensing platforms are based on the changes in electrical behaviour, for example, resistance, inductance, conductance and changes in semiconductor properties. These sensors come under the headings of chemiresistor and ChemFET.[5–7]

The detection of nitrous oxide (N_2O) in the environment is now of major concern, for the following reasons. It absorbs radiation from 550 to 650 cm^{-1} and from 1250 to 1350 cm^{-1}. It is therefore the third largest contributor to the greenhouse effect, behind CO_2 and CH_4.[12] In addition, N_2O has a global warming potential 300 times that of CO_2 over a 100 year time scale due to its longevity.[13] Additionally, N_2O is the largest stratospheric ozone-depleting substance and is projected to remain so for the remainder of this century.[14] Increasing levels of N_2O resulting from anthropogenic activities in agriculture such as the widespread use of fertilizers in rice paddies,[15,16]

[a]Non-linear Dynamics and Fiber Optics, Instituto de Óptica "Daza de Valdés" (IO-CSIC), Calle de Serrano, 121, 28006 Madrid, Spain. E-mail: T.Allsop@hull.ac.uk

[b]Aston Institute of Photonic Technologies, Dept. of Electronic Engineering, Aston University, Birmingham, B4 7ET, UK. E-mail: A.ROZHIN@aston.ac.uk

[c]Department of Engineering, University of Hull, Hull, HU6 7RX, UK

[d]Nanoscience Research Group, School of Engineering and Applied Science, Aston University, Aston Triangle, Birmingham, B47ET, UK

[e]Higher College of Technology, Al-Khuwair, PO Box 74, Postal Code 133, Sultanate of Oman

[f]School of Engineering, Computing and Mathematics, University of Plymouth, UK

† Electronic supplementary information (ESI) available. See DOI: 10.1039/d0na00525h

forest clearing, fossil fuel combustion[17] and denitrifying bacteria[18] are now a cause for alarm. The detection of N_2O is a challenging operation. Despite it being a thermodynamically potent oxidant, it is kinetically very stable and therefore behaves as an inert molecule. Field measurements typically are conducted using the "closed chamber method",[19] which has come under increasing scrutiny with regards to accuracy.[20] Therefore, there is a need to create a sensing platform to conduct field/*in situ* measurements with high sensitivity and a low detection limit, which is also simple to operate and regenerate, portable, robust, and power efficient for remote field measurements and data collection.

Current conventional methods are laboratory based, using surface chemisorption and gas chromatography with mass spectrometry.[21] Although having high sensitivity and ultra-low detection limits, they are not suitable for remote field measurements. Other sensing paradigms have been constructed based upon MOS sensors but these have poor chemical selectivity and detection limits from 10 ppm to 300 ppm. Such devices require relatively high regeneration temperatures that would be a challenge to the power budget of a remote stand-alone system.[22] There are absorption spectroscopy techniques using an Imaging Fourier Transform Spectrometer working in conjunction with laser illumination. Despite several examples of utilization of the infrared laser-absorption spectroscopy for field use, they usually have poor limit of detection of 0.1% of the ambient concentration for N_2O with a time response averaging hundreds of seconds. Other optical methods include multi-pass cells, high-finesse optical cavities, photoacoustic (PA) trace-gas detection and amperometric methods.[23,24] All these options display good detection limits ranging from 1 ppb to 40 ppb and response times in the tens of seconds, but all are hindered by their mechanical fragility and their inability to work remotely in the field. Therefore, they do not represent a practical solution to collect large sets of data, as needed for environmental studies. There are examples of electrochemical microsensor yielding a limit of detection of 0.04 ppm, from Revsbech's group at the University of Aarhus but it is an electrically based system and has got issues of polarisation.[24] Other optical methods include absorption spectroscopy using mid-infrared quantum cascade lasers[25] but these types of techniques yield poor detection limits for N_2O concentrations of approximately 0.1 v/v% and are not standalone remote systems. Furthermore, ZnO/Au nanostructures have been investigated recently as a possible 100 ppm sensing platform[26] using a combination of electrical properties (sensing range from 1 ppm to 5 ppm) and Raman spectroscopic analysis. The platform shows promise but it is still a laboratory based system using a high operating temperature of 150 °C, which is challenging for remote standalone system with regards power consumption.

In this paper, we demonstrate a new approach for the detection of specific gases under normal atmospheric conditions of 1 atm and 20 degrees C using an optical plasmonic sensing platform consisting of a 2-dimensional nanostructured topology, on the surface of which are adhered the carbon nanotubes (CNTs). Effectively, we are taking a conventional planar multi-layered film consisting of a top metal layer

followed by an insulator layer of SiO_2 with a bottom layer of germanium. The germanium is used in the process, involving UV irradiance, with the purpose of creating the nanowires of platinum. After the UV processing the germanium compacts and we produce a surface corrugation with the platinum at its apexes. As a result, Pt nanowires were created surrounded by air and SiO_2. This nanostructured array is produced by an advanced laser fabrication process commonly associated with fibre gratings (long period and Bragg gratings),[27] that creates and supports infra-red localised surface plasmons having spectral index sensitivities in excess of 10^4 nm per RIU, amongst the highest index sensitivities achieved.[28] The platinum nanowires support the Localised Surface Plasmons (LSP) that create infrared surface plasmon resonances in the optical transmission spectrum. As the refractive index changes at the platinum-surrounding environment interface, the spectral characteristics of the localised surface plasmon alters. The change in the refractive index is actually a variation in the permittivity which is dependent upon the electron density especially for metals, using Lorentz–Drude models of material permittivity.[29]

The optical sensing platform response to nitrous oxide is shown up to 100% atmosphere of nitrous oxide with a limit of detection of 109 ppm, a response time of seconds and with the possibility of regeneration. This plasmonic sensing platform directly monitors the changes in refractive index (the permittivity) caused by the chemical reaction of the polymer with the specific gas molecule and the CNTs itself. To the authors' knowledge, this is the first time CNTs and a plasmonic optical interrogation scheme have been used working in conjunction to detect N_2O, utilising the optical properties of the CNTs and not their electrical properties to make measurements. Thus, it can be used in flammable and potentially explosive environments due to the non-electrical and passive mechanism of the sensing platform.

There are two significant outcomes from this work. Firstly, the demonstration of infra-red plasmonic sensing platform working in conjunction with CNTs with an additional functional layer polyethyleneimine polymer (PEI) to enhance the spectral response for N_2O gas molecules. The addition of the CNTs modifies the overall composition of the nanowires transforming the overall optical properties of the nanowire. Thus the LSP spectral response to refractive index changes, this case, increasing spectral sensitivity. This transformation and increase in spectral sensitivity to index is shown in the experimental results. Furthermore, the addition of PEI to the local environment of the Pt + CNT nanowires changes the optical properties and response to the larger surrounding environment. The addition of PEI creates excess of electrons on the CNTs' sidewalls. This makes an efficient electron transport from CNT–PEI to N_2O, thus changing the local permittivity (effective refractive index) and amplifying the spectral response of the surface plasmon.

Secondly, the use of CNTs with a simple optical sensing/interrogation platform that is akin to MOS sensors but with the attribute of higher chemical selectivity. Furthermore, this sensing approach has the potential for sensing of other harmful

compounds, due to the existence of a myriad of protocols for CNTs functionalisation, and can be utilised for multiple detection by forming sensing arrays. Due to the size and the interrogation scheme used, the system can be made portable with a low power budget so it can be used as a standalone and remote system. The sensing approach reported here has a great potential to be used remotely at various locations in the natural environment along with having good chemical selectivity and reasonable good sensing performances that are usually associated with laboratory based equipment. The sensing approach shown in this article as a with a limit of detection of 109 ppm which is comparable to or better than most MOS sensors[8–10] with the major advantage of room temperature regeneration, ideally for remote sensing unlike MOS sensors that require relatively high regeneration temperatures and thus having major issues with regards power budgets for remote sensing. Furthermore, the sensing approach demonstrated here has shown chemical selectivity against other greenhouse gases carbon dioxide and methane. In addition, the a response time of ~19 s seconds which is very good compared to a few 10 s to 100 s seconds of the other methods stated in the paper. These sensing attributes are critical for the monitoring and collection of huge datasets to help environmentalist in their analysis of nitrous oxide's impacts on ecosystems.

2. Experimental

2.1 Fabrication of nanostructured plasmonic sensing platform

The design and fabrication of the nitrous oxide sensing platform is a multi-stage process with the device's spectral behaviour characterised at each fabrication stage, the fact is that device's optical properties changes due to different optical mechanisms at the different stages.[28–31] The initial stage is the lapping of a standard telecoms optical fibre (SMF28) that creates a D-shaped fibre with the flat area 3 microns from the core/cladding interface as shown in Fig. 1a, these lapped D-

shaped fibre are purchased from Phoenix Photonics Ltd, UK. The second stage is the deposition of three different material thin films (germanium (48 nm), silicon dioxide (48 nm) and metal over layer coating of platinum (28 nm)) using RF sputter (Nordico 6 inch RF/DC 3 target excitation machine, Nordiko Technical Services Limited, Havant, Hampshire, UK). The purpose of using platinum is to maximise the index spectral sensitivity of the surface plasmons in the gaseous regime.[28] This stage creates a conventional surface plasmons sensing device. The final stage of fabrication is the nano-patterning by ultraviolet (UV) argon-ion laser (Sabre Fred, Coherent Inc.) irradiance at 244 nm, which is achieved using a phase mask usually applied to inscribe Bragg gratings into optical fibres.

The characterisation of the plasmon devices includes polarisation dependence, temperature sensitivity and refractive index sensitivity, both in aqueous and gaseous index regime and carried-on with the experimental apparatus shown in Fig. 1b and c.

The aqueous refractive index characterisation is done by immersing the surface plasmon resonance/localised surface plasmon SPR/LSP fibre device into certified refractive index liquids (Cargille-Sacher Laboratories Inc.) with a given accuracy of ± 0.0002.[32] For this purpose, the device is placed into a V-groove on an aluminium plate, which is machined flat to minimise bending of the fibre, since this can affect the experimental results due to the polarisation dependence of the SPRs and LSPs. The plate was placed on an optical table, which acted as a heat sink to help maintain a constant temperature throughout the experiments. The plasmonic devices are illuminated with polarised light, such that the polarisation state of the light yields a maximum coupling to plasmons producing a maximum optical strength of the plasmons' resonance in transmission spectrum. This is achieved by using a broadband light source ((Agilent 83437A Broadband light source with four edge-emitting LEDs with central wavelengths 1310 nm, 1400 nm, 1550 nm and 1650 nm)) in conjunction with a broadband linear polariser (polarimeter (Tektronix, PAT 9000B)) along with polarisation controller. An in-line polarimeter (General Photonics, Polarisation Analyser, POD-201) is used to monitor the polarisation and to ensure that polarised light as good linearity and constant over the wavelength range used to observe the surface plasmon reasonances 1300 nm to 1670 nm.

The gaseous refractive index regime spectral characterisation is achieved by effectively replacing the V-groove with a gas chamber as shown in Fig. 1c. The inlet sparge of the gas chamber is connected to a gas manifold, which is connected to a series of gas cylinders via a series of isolation and control valves. The gases used for gas index characterisation are the alkane gases (methane, ethane, propane and butane) due to their similar chemical properties to each other. In addition, the temperature spectral sensitivities were investigated by replacing the V-groove holder with a thermal Peltier situated inside an insulated box.

The central wavelength of the extinction surface plasmon resonance transmission spectrum is calculated by the first moment of the power spectrum: the centroid by geometric decomposition.[33] The centroid is given by:
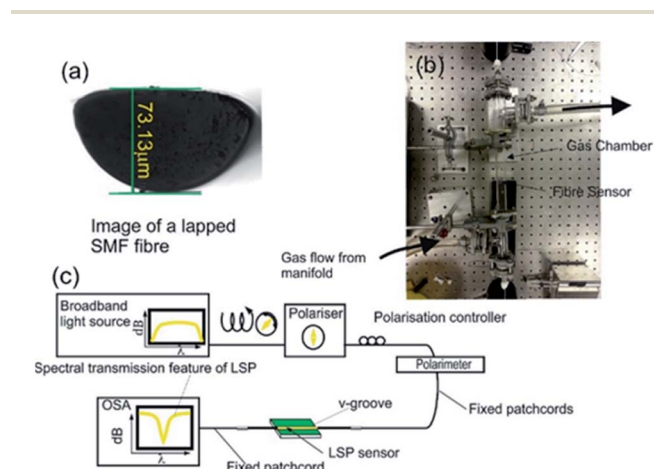

Fig. 1 (a) Microscope image of the cross-section of the D-shaped fibre used in the fabrication process. (b) The gas chamber used to replace the V-groove for refractive index sensitivity in the gaseous regime. (c) A general schematic of the characterisation apparatus used.

$$\lambda_{\text{cent}} = \int_{\lambda_f}^{\lambda_s} \lambda I(\lambda) \mathrm{d}\lambda \bigg/ \int_{\lambda_f}^{\lambda_s} I(\lambda) \mathrm{d}\lambda$$

where λ_{cent} is the centroid wavelength over a range from λ_s to λ_f and $I(\lambda)$ is the associated amplitude/intensities measured in dBs as a function of wavelength over the part of the transmission spectrum where the extinction surface plasmon resonance is spectral located. The intensity value chosen to define the wavelength range λ_s to λ_f is the points at -1 dB of the transmission spectrum of the extinction surface plasmon resonance. The associated centroid strength value is calculated as the mean value over the same interval range of λ_s to λ_f.

2.2 SWNTs dispersion preparation

HiPco type of single wall carbon nanotubes (SWNTs) were purchased from Carbon Nanotechnologies Inc. (lot no. PO279) and used as source material. The HiPco process produces SWNTs with a broad range of nanotube diameters leading to the broad absorption bands of these nanomaterials. Dispersive solution of HiPco SWNTs is prepared with N-methyl-2-pyrrolidone (NMP) organic solvent at nanotubes concentration of 0.1 mg mL^{-1}. Initial SWNTs dispersion is prepared by ultrasonication using NanoRuptor (Diagenode) processor for 1 hour at 21 kHz and 250 W to obtain homogeneous dispersion. Then, the resulting mixture was ultra-centrifuged with Beckman Coulter Optima Max-XP for 1 hour at 17 °C using MLS 50 rotor at 30 000 RPM to remove impurities and residual bundles. The top 50% of the final dispersion is used to carry out this study.

The LSP device is then coated with PEI solution 50 wt% in H$_2$O (PEI, sigma Aldrich, lot no. MKBS7391V) and left in the oven at 50 °C overnight. It is well-known that PEI polymer has a p-type behaviour due to the adsorption of O$_2$ from the ambient and that each O$_2$ molecule withdraws $\sim$1/10 of an electron from the SWNTs.[34] After PEI adsorption, the SWNT layer exhibits clear n-type FET characteristics.[35]

3. Results and discussion

3.1 Nanostructured plasmonic sensing platform

The nanostructured material used as the optic plasmonic sensing platform is created using three materials. These materials and thickness, in order of deposition are germanium (48 nm), silicon dioxide (48 nm) and an over layer coating of platinum (28 nm), see Fig. 2a. More detail with regards equipment is given in the ESI section.†

The nano-patterning occurs during the UV processing, two physical mechanisms happen within the coating and specifically with germanium and its oxides. Firstly, a change in the electron density of specific Ge=O/Ge–O bonds, effectively a redox reaction, thus altering the permittivity and therefore the refractive indices. Secondly, a structural change in the material occurs that results in geometric spatial compaction, creating stress–strain in the material.[36,37] This second "compaction" mechanism gives rise to the formation of spatial geometric surface physical features creating a 2-dimensional nano-patterned structured material. A more detailed account of this

Fig. 2 (a) The fabrication procedure and materials used (Ge–SiO$_2$–Pt) and appearance of the plasmonic devices. (b and c) A microscope image of a section of coated (coating Ge–SiO$_2$–Pt) D-shaped fibre that has been UV processed, with a magnified inset to show the surface corrugation. (d) An AFM topological map showing a typical surface of the material before and after UV exposure (germanium, silicon dioxide, platinum).

This journal is © The Royal Society of Chemistry 2020

direct-write UV-chemically induced geometric inscription technique can be found elsewhere.[38]

The surface topologies were studied using optical microscopy, see Fig. 2b and c, and an atomic force microscope (AFM), see Fig. 2d. Firstly, the microscope images demonstrated that the fabrication technique creates long-range repeatable structural order, 100 μm shown in Fig. 2c, with an overall scale of the order of centimetre, typical long range order distances are 100 μm which is an important factor for overall sensitivity. Secondly, Fig. 2c, shows more detail of the individual nano-antennae. An example of the AFM map is shown in Fig. 2d showing the surface topology before and after UV processing. In the "Pristine condition" before UV processing, the Pt is planar film on the top of SiO_2 and supported by a layer of Ge. After UV processing, the "UVed material" is an alternating ridges and grooves on the D shape fibre surface, and the platinum is located at the vertices of the corrugation creating Pt nanowires surrounded by air and SiO_2. The surface topology consists of an array of parallel nano-antennae of the metal used in the overlay film with the dimensions of an individual nano-antenna being typically a mean radius of 130 nm, length of 20 μm and the array lengths of the order of 2 cm (see ESI section†).

The film thicknesses are chosen to produce efficient surface plasmon coupling at wavelengths of approximately 1.5 μm in order to maximise the surface plasmon field for the gas index regime resulting in the greatest refractive index spectral sensitivity. More details on localised surface plasmon (LSP) fabrication can be found in ref. 28, 30 and 31. Moreover, these structures enhance overall spectral sensitivity of these infrared surface plasmons by increasing the interaction length of the surface plasmon with its surrounding environment (work submitted for publication).

3.2 Carbon nanotubes

The two types of nanostructured plasmonic fibre device were created, one with just the carbon nanotubes and secondly the carbon nanotubes coated with polymer. The general process used to adhere the carbon nanotubes is to immerse the fibre into solutions containing the single wall carbon nanotubes (SWNTs). This process is broken into three sections as described below: (i) preparation and characterisation of the dispersion of SWNTs in NMP organic solvent; (ii) the adhesion of the SWNTs to the fibre; (iii) the applying of the functionalising polyethyleneimine (PEI) polymer on a resulting SWNTs-LSP structure by a simple dip coating method.

Absorption and PhotoLuminescence Excitation-emission (PLE) spectroscopy studies were conducted on a sample SWNTs dispersion along with Raman spectroscopy, see Fig. 3. The PLE data (Fig. 3a) implies that there is a large fraction of semiconducting SWNTs[39] in the dispersion. In addition, Fig. 3a and b confirm a broad resonant absorption of the E11 transition of the HiPCO SWNTs centred around 1000–1300 nm. Consequently, Fig. 3a and b also confirm that the majority of the nanotubes in the device will not contribute to the resonant absorption of the N_2O gas. Fig. 3c presents Raman spectrum for SWNTs dispersion used in this study. According to the Kataura plot,[40] excitation wavelength of 532 nm matches the M11 transition of m-SWNTs. This is supported by the Breit–Wigner–Fano (BWF) line shape of the G band. The key features in the Raman spectrum of SWNTs are the radial breathing modes (RBMs, 150–300 cm^{-1}), the D (disorder, ~1329.5 cm^{-1}), G (graphite, ~1591.1 cm^{-1}) and 2D (~2633.3 cm^{-1}) bands. The RBMs correspond to low-frequency vibrations of carbon atoms in the radial direction and are highly sensitive to the diameter and chirality of SWNTs. There is one dominant RBM in the spectrum of the SWNT centred at 273.6 cm^{-1}, corresponding to a nanotube with a diameter of 0.88 nm.[41] Moreover, the "splitting" of the G mode indicates that metallic SWNTs are present along with the semiconductor SWNT, see Fig. 3c.

A dispersion of SWNT containing a mixture of metal and semiconductor tubes was poured into a micro-capillary tube holding the surface plasmon fibre device and left for one hour. Finally, the device was dried in air at room temperature for 10 hours.
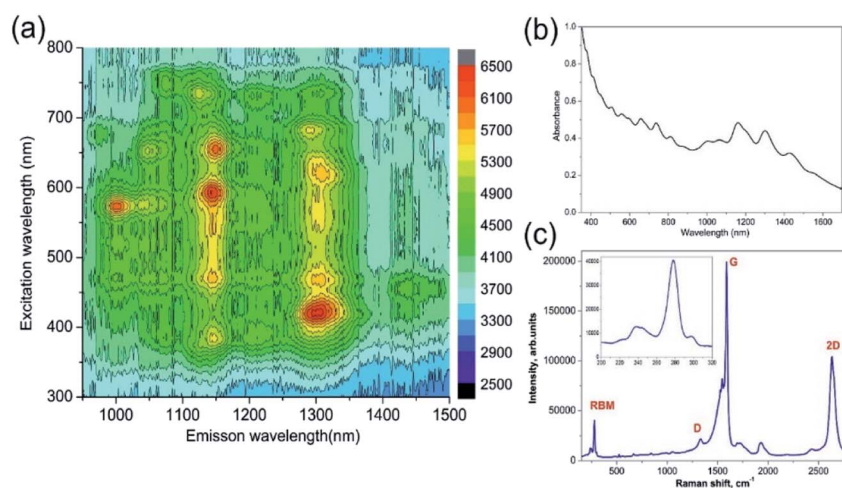

Fig. 3 Spectroscopic analysis of the SWNTs coated plasmonic fibre with N-methyl-2-pyrrolidone as the dispersion media (a) photoluminescence excitation-emission map of excitation wavelength and the observed emission spectra (b) absorption spectra. (c) Raman Spectroscopy at 532 nm excitation.

3.3 Aqueous refractive index regime

Fig. 4 demonstrates the improvement in the index spectral sensitivity achieved with the nano-structuring of the thin film material. The first observation of the spectral index sensitivity shows blue shifts (Fig. 4b and c) before and red shifts (Fig. 4e and f) after UV processing. This spectral behaviour relates to the changes that occur in the material during UV exposure from a flat planar coating of platinum before UV processing (pristine) to a corrugated coating UVed material, see Fig. 2d. This surface topology transformation is due to direct-write UV-chemically induced geometric inscription based upon the spatial structural changes of Ge, a geometric compaction of material brought about by its interaction with UV laser light.[31,34] This transforms the platinum planar surface to an array of platinum nanowires, thus modifying the conventional surface plasmon (CSP) to localised surface plasmons (LSP) that have different dispersion relationship to those of the CSP. The LSP spectral behaviour/dispersion relationship is very much dependent upon the individual shape and size of the nanowires along with the overall surface topology, such as period, and this dictates the spectral index sensitivity and whether the wavelength shift of the resonance is either blue or red.[42,43]
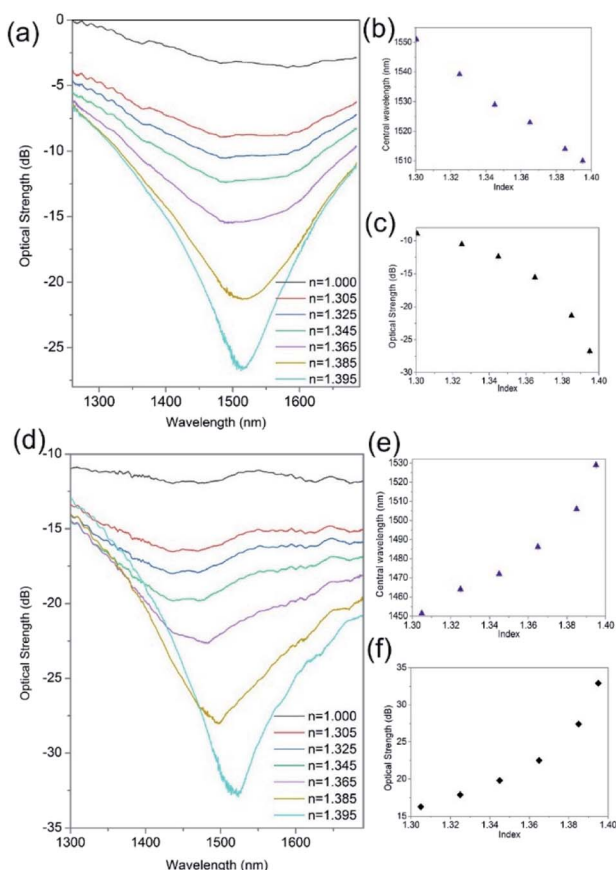
The change in index sensitivity for the same $Ge/SiO_2/Pt$ device before UV processing shows maximum sensitivities of 400 ± 10 nm per RIU and 500 ± 10 dB per RIU (Fig. 4a–c). After UV processing, a maximum refractive index sensitivity 2200 ± 60 nm per RIU and 700 ± 10 dB per RIU is obtained (Fig. 4d–f), which shows an increase of a factor of 4 and can vary up to a factor of 10. This is due to the imperfections in the fabrication processing (alignment of fibre and laser spot, delivery of optical energy, *etc.*) at present. Also it was found that the polarisation dependence and sensitivity increases with UV processing, from 1.4 nm per degree to 5.3 nm per degree and the corresponding optical strength sensitivity increased from 0.9 dB per degree to 6.3 dB per degree. These properties and time response are investigated after the final stage of fabrication.

3.4 Gaseous refractive index regime

The gas index sensitivities where determined by replacing the V-groove with a gas chamber and a typical example for the 2-dimensional nano-structured LSP fibre device is shown in Fig. 5. The sequence of gases and measurements are as follows: air (an initial measurement), methane, ethane, propane and butane. The flow rate for the experiments is 3 litres per min and the exhaust sparge of the gas chamber is connected to inflatable gas bag (capacity 5 litres). A flow meter is used to maintain a constant flow rate and the gas to be used for the next set of measurements is also used to purge the gas apparatus (total volume 1.5 litres) of the previous gas, after the gas bags are full, five measurements are taken and the process is repeated another two times (Fig. 5b). By inspecting Fig. 5a, c and d, the average (central wavelength) and maximum spectral wavelength index sensitivities, assuming linearity, are -530 ± 26 nm per RIU (Fig. 5c) and -2100 ± 40 nm per RIU (wavelength for air is 1425.5 nm and butane is 1422.9 nm, see Fig. 5a) and the intensity index sensitivities are -2900 ± 80 dB per RIU (Fig. 5d)

Fig. 4 An example of the variation in refractive index sensitivity of a $Ge/SiO_2/Pt$ fibre plasmonic device. Before UV processing (a) the transmission spectra as a function of index, (b) central wavelength (c) optical coupling strength. After UV processing (d) the transmission spectra as a function of index, (e) central wavelength (f) optical coupling strength.
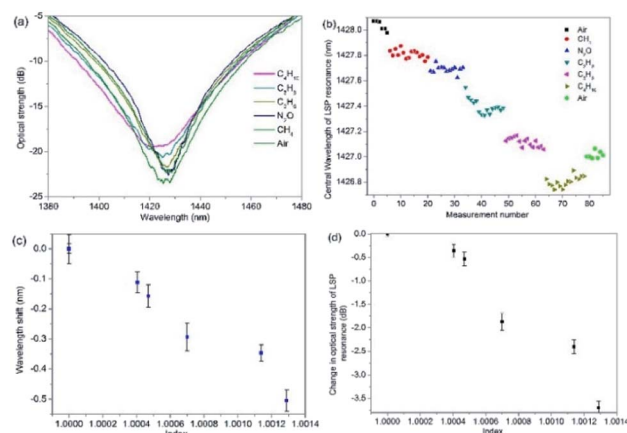

Fig. 5 Typical experimental gas index regime results with UV processed $Ge/SiO_2/Pt$ device (a) the transmission spectra as a function of different gases (b) the individual measurements of the central wavelength of the LSP resonance for each gas from the experiments. (c and d) The wavelength and optical strength sensitivity as a function of the different refractive indices of the alkane gases and nitrous oxide, respectively.

and -4100 ± 100 dB per RIU (optical strength for air is 23.9 dB and butane is 19.0, see Fig. 5a).

The error for sensitivity are obtained from the variations in the experimental data for each test, the variations in wavelength can be seen for gas in Fig. 5b.

Furthermore, the experimental data in Fig. 5b, shows a spectral drift of ~1 nm between the initial and final measurement of air. This thermal spectral drift is due to the room temperature gradually decreasing over the time of the experiment, by 2 °C. This was a gradual change and was found to be linear over the time of the experiments. In addition, Fig. 5c and d have had this time dependence removed from the data, this process is repeated in proceeding experimental data shown in Fig. 6 and 7. Furthermore, the N_2O was also used in this experiment the plasmonic sensing platform produced a wavelength shift of -0.15 nm which is expected due to the refractive index of N_2O itself.

3.5 The sensing of nitrous oxide gas

The gas index sensitivities where determined for the 2-dimensional nano-structured LSP fibre devices. After the adhesion of the SWNTs and SWNTs plus PEI, the two types of gas sensing devices were placed into the gas chamber and the above gas sensing procedure was repeated with the addition of nitrous oxide and carbon dioxide. The experimental data shown in Fig. 6 are typical results for LSP fibre device coated with the SWNTs. Fig. 6b shows that there is a small spectral drift of the LSP resonance of 0.07 nm caused by the drop in the ambient room temperature of the laboratory from 26.6 to 25.6 degrees C, which accounts for the drift, all the alkane gases produced a red wavelength shift in the resonance. It is assumed that this red shift is due to the increase in the surrounding medium's refractive index, with the propane to butane producing
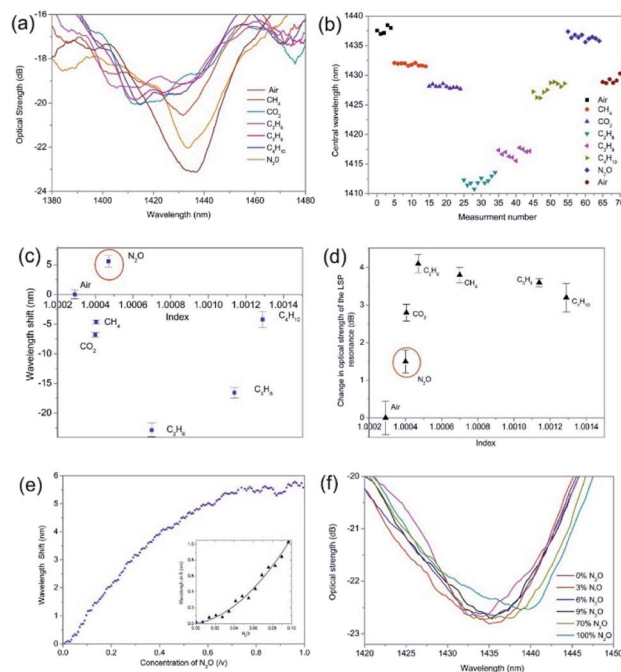

Fig. 6 Typical experimental results of an UVed Ge/SiO$_2$/Pt LSP fibre device coated with SWNTs as a function of surrounding refractive index and nitrous oxide (a) the transmission spectra as function of surrounding gas. (b) The individual measurements of the central wavelength of the LSP resonance for each alkane gas and nitrous oxide (c) and (d) the wavelength and optical strength sensitivity as a function of the different gas's refractive index respectively.

Fig. 7 The typical experimental results of a UV processed Ge/SiO$_2$/Pt LSP fibre device coated with SWNTs and PEI as a function of surrounding refractive index and the detection of nitrous oxide (a) the transmission spectra as function of changing surrounding index and the nitrous oxide. (b) The individual measurements of the central wavelength of the LSP resonance for each alkane gas and nitrous oxide (c) and (d) the wavelength and optical strength sensitivity as a function of the different gases and their refractive index respectively. (e) The wavelength response to increasing N$_2$O concentration, the insert showing the wavelength shift with low concentrations of N$_2$O. (f) Examples of the changes in transmission spectra of LSP resonance to various concentrations of N$_2$O as a percentage of total volume.

a wavelength shift of $+0.38$ nm which leads to a spectral index sensitivity of $+2534 \pm 25$ nm per RIU and $+3545 \pm 28$ dB per RIU.

Also, the N_2O showed a wavelength shift of -0.11 nm and -0.01 dB, giving sensitivities of -611 ± 31 nm per RIU and -66 ± 12 dB per RIU with respect to changes from air. The nitrous oxide produced a blue wavelength shift, which implies that the permittivity of the SWNTs is reduced, suggesting the N_2O has produced a REDOX reaction with SWNTs. Furthermore, if the change in wavelength was purely due to changes in refractive index we would expect to see a red wavelength shift similar to what was observed with just the plasmonic sensing platform seen in Fig. 5. It is known that SWNTs can help in the decomposition of N_2O, converting toxic N_2O to a nontoxic N_2 molecule and SWNTs are being considered in some catalytic applications.[35] Moreover, other researchers have suggested that the N_2O molecule acts as the electron deficient molecule while the SWNT acts as the electron donor. Thus, electrons will be transferred from the SWNT to N_2O in order to undergo the decomposition process. The shorter the bond is, the higher the electron density is in the local bond. Hence, the higher electron density in the C1–C2 bond of the SWNTs should aid the cycloaddition reaction with incoming N_2O.[35,44,45] Therefore, this
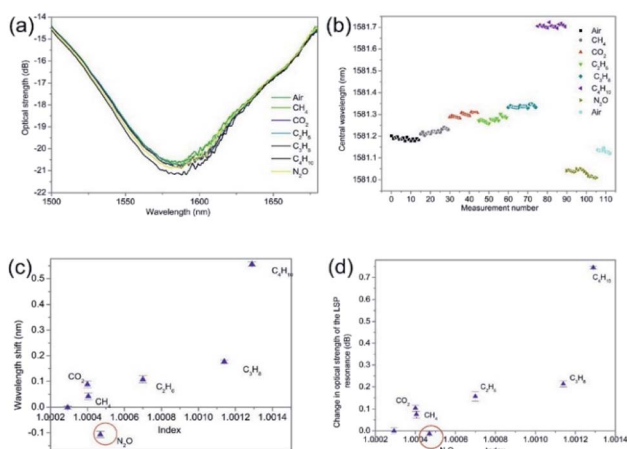
would lead to reduction in the electron density and thus a lowering of the permittivity, leading to the lowering of the effective refractive index. This should be experimentally observed as a blue wavelength shift, as it is confirmed in our LSP devices. Furthermore, the authors have observed a similar spectral behaviour with Pt/ZnO composite material in the past.[46] Moreover, this is also consistent with the carbon dioxide results shown in Fig. 6 that produces red wavelength shifts; +0.14 nm, that indicates an increase in permittivity, which was previously observed by the authors.[47]

A second series of experiments were conducted on a UV processed LSP fibre device coated with the SWNTs and with the addition of the PEI polymer. The gas regime of index sensitivity and the effective detection of N_2O are shown in Fig. 7. By analysing the experimental results, it was found that the PEI amplified the wavelength shifts and optical strength changes with maximum blue wavelength shift of -22 nm and -1.7 dB for ethane. Specifically for the N_2O, there was an amplification in the overall wavelength shift associated with N_2O but it is a red wavelength shift $+5.7$ nm and increase in optical strength of $+2.9$ dB compared to the previous experiments. The temperature was also monitored over the tests and a 3 °C increase was observed. Furthermore, the addition of the PEI has also yielded a maximum negative spectral response for ethane from air, which is the equivalent of $5.6 \times 10^4 \pm 400$ nm per RIU and -4200 ± 80 dB per RIU including experimental errors. The detection of the N_2O yielded a spectral sensitivity of $+3.1 \times 10^4 \pm 350$ nm per RIU and $+1.6 \times 10^4 \pm 200$ dB per RIU. The spectral response of the sensor to CO_2 showed a blue wavelength shift of 7 nm, matching that of the alkane gases, demonstrating an increase in permittivity. Furthermore, the magnitude of the CO_2 shift is significantly more than that of CH_4, thus proving that the presence of PEI is increasing the sensitivity of the sensor to CO_2.

The temporal response of the sensors were estimated from measurements made of the wavelength and intensity variations using an optical spectrum analyser, OSA, (86145A Agilent Optical Analyser, resolution 0.06 nm, accuracy 0.05 nm), on which the transmission spectrum information appears instantaneously for each scan datum point to the next datum point. The minimum response time, as indicated by the OSA is then indicatively the maximum response time of the sensor.

Thus, to estimate the temporal response of the scheme we need to observe the time taken to acquire the section of data that represents transmission spectra of the LSP needed to detect those spectral changes with respect to changes in the concentration of nitrous oxide.

As previously stated, the gas flow rate is maintained at 3 litres per min by means of a flow control meter. The volume of the chamber system is 1.5 litres, so to change the atmosphere within the chamber requires approximately 60 seconds. Furthermore, the time needed to obtain a complete transmission spectrum of the plasmonic fibre sensor with a bandwidth of 100 nm requires an OSA scan time of 19.08 seconds for a complete spectral transmission. Thus a completed transmission scan, examples shown in Fig. 7a, represents a 32% change in gas volume within the chamber over one scan. Each

scan consists of 1000 spectral datum points, thus using a 100 nm spectral bandwidth yielding a scan resolution of 0.1 nm and a time per spectral datum point of 0.019 seconds.

Using the same approach that is used to calculate the centroid at the optical strength of -1 dB of the extinction surface plasmon resonance transmission spectrum. The air resonance to the nitrous oxide resonance of the sensor is approximately 100 nm, (see Fig. 7a) then the slowest response time is 19.08 seconds but this is dependent upon the interrogation scheme adopted and dependent upon how much of the bandwidth of the surface plasmons resonance transmission spectral feature is interrogated.

The first general observation is that the spectral position of the resonance and its optical strength change at each stage of fabrication of the fibre optic LSP gas sensor. Thus, the central wavelengths of resonance and its optical strengths for each step are (1) the LSP fibre device is 1428.0 nm and 24 dB, (2) the LSP and the SWNTs fibre device 1581.2 nm and 21.2 dB, (3) the LSP, SWNT, and PEI fibre device 1437.6 nm and 23.2 dB.

Furthermore, the associated errors for measurements can be seen in the perspective Fig. 4, 6 and 7. It is expected that the resonances and coupling strength would change for each step in the process for the following reasons. Firstly, the addition of the SWNT layer would change the overall waveguide structure adding new material with its own permittivity and dispersion properties and thus changing the resonance condition and coupling strength resulting in new overall spectral transmission features (peak strength, central wavelength and full-width at half-maxima). The simplistic mathematical model that looks at the plasmons that exist at a metal–dielectric interface for two homogeneous semi-infinite media yields a dispersion relation that produces a propagation constant of the plasmon of

$$k\sqrt{\frac{\varepsilon_m(\lambda)n_s(\lambda)^2}{\varepsilon_m(\lambda) + n_s(\lambda)^2}}.$$

The parameters are defined as: k the free space wave number, ε_m the dielectric constant of the metal film or the "effective" dielectric constant and is real and complex; ($\varepsilon_m = \varepsilon_{mr} + \iota\varepsilon_{mi}$) and n_s is the refractive index of the surrounding medium.[41] Furthermore, in the fabrication process of the LSP devices ε_m becomes more complicated with the additional layers changing the optical properties of the specific metal layer that generates the localized surface plasmons. The underlying principles of the modelling are the same but additional factors become important, such as, surface topology.[42,43]

The experimental data displayed in Fig. 7 demonstrates clearly the effect of integrating 2-dimensional nanostructured material (both the plasmonic LSP platform and the SWNTs) with polymer PEI. It is well known[35] that the deposition of a PEI polymer leads to the creation of an effective n-type conductor *via* donation of PEI's electrons on SWNTs sidewalls. Thus the CNT–PEI system has an excess of electrons, which then efficiently transferred from the tubes to chemically adsorbed N_2O molecules. This yields an enhanced selective spectral sensitivity for N_2O. The purpose of the nano-antennae/nanowires is to

amplify the wavelength shift and the change in the optical strength for the detection of N_2O. The results show, firstly, that a wavelength shift occurs from −0.11 nm full-scale deflection. (FSD) to +5.7 FSD (Fig. 7c), a factor of 54 increase in magnitude, resulting in the largest equivalent gas-index sensitivity of −5.6 × 10^4 nm per RIU compared to other sensors. Secondly, the optical strength changes from −0.01 dB FSD to −2.9 dB FSD, an increase factor of 290 (Fig. 7d). Fig. 6e shows that saturation occurs at 80 v/v%, (ratio volume of N_2O to total volume available). Assuming a linear response over a range of 10% to 70% (v/v%) the sensor yields a sensitivity to N_2O concentration of $\Delta\lambda/\Delta$[N_2O] = +10.47 nm/(v/v%) and a working resolution of 87 ppm.

An important parameter in sensing is the limit of detection (LOD) which depends on the interrogation scheme, the light source spectral width that leads to a finite wavelength resolution of light source, and the noise bandwidth of the measuring system. The LOD can be expressed in terms of standard deviation of noise of the sensor output $\Delta\lambda_{error}$, bulk sensitivity defined as $S_{\lambda B} = \Delta\lambda/\Delta n_s$ and bandwidth of the spectral transmission feature of the surface plasmons resonance $\Delta\lambda_{feature}$.[48]

$$LOD = \sqrt{\frac{2(\Delta\lambda_{feature} + \Delta\lambda_{error})}{1000}} \Big/ S_{\lambda B}.$$

Firstly, $\Delta\lambda_{error}$ is estimated from the variance of the difference from the expected values obtained from a second order polynomial curve fit to the experimental data. Furthermore, there are 1000 discrete spectral data points per spectral scan across the resonant peak. Therefore, the full-width at a half-maxima of bandwidth resonances gives 15.2 nm and the standard deviation from the expected value to the experimental data yields 0.015 nm and average spectral sensitivity of 15.9 nm/(v/v%) of the initial concentrations. This yields a limit of detection of 109 ppm estimated by a second order polynomial curve fit, shown in the insert of Fig. 7e.

Thirdly, the N_2O yields the opposite wavelength shift to that of the alkane gases, thus providing a specific gas detection system for nitrous oxide, see Fig. 6c and 7c. Using just the SWNTs gave a reduction reaction with N_2O, which is documented in the research literature[35,44,45] and is consistent with experimental results observed with another type of SWNTs and another REDOX reaction with carbon dioxide.[46]

The addition of the PEI created a change in sign of the wavelength shift produced by the N_2O or alkane gases. There are several possible reasons for this spectral behaviour. Firstly, the PEI is a cationic polymer[49] and the N_2O has an uneven charge distribution ($N{\equiv}N^+\text{-}O^- \leftrightarrow {}^-N{=}{}^+N{=}O$). Therefore deprotonation/protonation can occur, thus effectively creating a reduction in the effective dielectric function of the surrounding medium of the LSP. These changes in spectral behaviour are to be expected. The addition of SWNTs will change the overall composite of the Pt nanowire to Pt + SWNT nanowires then to Pt + SWNTs + PEI nanowires leading to a modification of LSP's optical properties response to refractive index. This can be thought as the change in the effective dielectric function of the nanowire in the framework of effective medium approximation using a Bruggeman approximation or a Maxwell–Garrentt approach;[50] the effective refractive index is given by the fractional volume of each component making up the nanowire. Furthermore these additional materials change the geometry "the shape" of the nanowires resulting in modification of the resonance condition and optical properties of the surface plasmons, and their dispersion relationships.

This suggests that the dispersion properties of the LSP have been altered by the presence of the PEI, resulting in the reduction of the permittivity which produces the observed red wavelength shift. Therefore, the blue wavelength shifts observed with the alkane gases represent an increase permittivity, with a maximum effect with ethane. A possible explanation for the experimentally observed maximum for ethane involves the chemisorption properties of the PEI, which has been used as a specific chemical adsorbent[51,52] and is a popular choice for carbon dioxide that has an effective kinetic molecular diameter of ∼330 pm which is similar to methane and ethane (both have ∼380 pm, increasing to ∼430 pm for propane,[53,54] and ∼450 pm for butane[55]). The smaller molecules can ingress into the PEI polymer with ethane, having the largest kinetic molecule setting a limit, effectively acting as a filtering process. Therefore, the effective dielectric function of the surrounding medium of the sensing platform increases as a function of molecular size and number of molecules that ingress into the PEI.[56]

It is useful to consider the chemical selectivity of the LSP sensing scheme. Firstly, comparing the SWNT coated LSP sensor results for N_2O to the results shown in[47] for CO_2 shows an opposite central wavelength shifts, −0.15 nm and +3.8 nm, respectively and importantly the N_2O has a net reduction in permittivity, hence the blue wavelength shift as shown in Fig. 6. Inspecting the transmission spectra in Fig. 7a, the peak resonant wavelength for CO_2 is 1413.25 nm and N_2O is 1433.88 nm. This spectral bifurcation of the resonance will allow detection of the presence of both CO_2 and N_2O in the same atmosphere by using two distributed feedback (DFB) lasers with light generation adjusted in resonance with both chemicals. The response of the PEI + SWNT coated LSP sensor to CO_2 of a blue wavelength shift the same as alkane gases, again is consistent, the net change in the wavelength is very much reduced, see Fig. 7. This desensitisation may be due to the excess of charge already present due to the PEI being a cationic polymer. It is known that PEI can function as a selective membrane, which allows nitrous oxide gases but blocks basic gases, such as NH_3.[57] The effect of humidity was not considered in these experiments. The initial air in the chamber was not dried nor was the air used to purge the gas chamber system. However, the results obtained were consistent from day to day.

Further observation: in all the experiments, from start to finish we observed spectral drifts. The net spectral drift with just the $Ge/SiO_2/Pt$ device was typically ∼1 nm over a period of 1 hour, (Fig. 4b), which reduced to typical values of ∼0.1 nm for the $Ge/SiO_2/Pt$ fibre device coated with SWNTs, (Fig. 5b) and ∼7 nm with the $Ge/SiO_2/Pt$ fibre device coated with SWNTs and PEI, (Fig. 7b). There are several factors that could be responsible for these drifts. The thermal optic properties of the materials change the spectral location of the resonant condition. Also the thermal conductivity and thermal expansion coefficients that

create spatial changes in the surface topology, thus changing the resonant condition. Furthermore, this also creates strain in the material, which in turn affects the polarisation state of the light, thus again changing the resonant condition. Moreover, the optical fibre used to create these devices is conventional single mode fibre with a cut-off at 1310 nm and is not polarisation maintaining fibre, thus small changes in the room temperature will contribute to the spectral drift of the surface plasmons' resonances but this would be a system error. Just considering the thermal properties, these effects appear to be consistent with the material constants of the coatings and the observed wavelength shifts of the different LSP devices. It was noted that the room temperature increased by approximately 1 °C per experiment, yielding temperature sensitivities of 1 nm C^{-1}, 0.1 nm C^{-1} and 2.3 nm C^{-1} for the LSP device, SWNT + LSP device and PEI + SWNT + LSP device respectively. It was also noted the wavelength shift to temperature is a linear dependence.

The smallest net drift is with the LSP device coated with SWNTs that has small thermal conductivity; 0.1 W m^{-1} K^{-1} (ref. 57) and has a negative thermal expansion coefficients $\sim -7 \times 10^{-6}$ K^{-1} (ref. 58 and 59) that is counteracting the positive thermal expansion coefficient of the germanium (+5.9 × 10^{-6} K^{-1}), platinum (+9.0 × 10^{-6} K^{-1}) and the silicon dioxide (+0.55 × 10^{-6} K^{-1}). Secondly, the LSP device yielded the second largest spectral drift and the LSP device coated with the PEI yielded the largest spectral drift. PEI has the thermal expansion of +56 × 10^{-6} K^{-1} (please see Goodfellows website regarding thermal expansion data).[60,61]

A general comparison can be made with the existing sensing platforms, as shown in shown in Table 1. The authors would like to remind the reader that this is not a review paper, thus the Table 1 gives a general overview of typical performance characteristics of available technologies. CNT chemiresistor and chemical field effect transistor (ChemFET)[5] respond to electrical changes and have detection limits ranging from 6 ppm to 1000 ppm that are similar to the 2-dimensional nanostructured material used in this paper. MOS sensing schemes have similar limits of detection from 10 ppm to 300 ppm, but suffer from poor chemical selectivity.[22] A further observation is that the time response of the LSP device is, in general, faster and in addition, this sensor has a room temperature regeneration unlike the majority of schemes reported along with similar limits of detection. Furthermore, the target molecules for the device described here is nitrous oxide Table 1 shows examples for nitrous oxide and the other oxide states of nitrogen.

Most of these sensing schemes are electrically based and would need high regeneration temperatures that would be a challenge for power budget requirements for remote standalone systems[17] and would not be suitable for many applications in flammable and explosive environments. Further reading on general performance is available in ref. 23. Additionally, Raman spectroscopic analysis produces spectra depending on the concentration of N_2O at room temperature,[26] but this is a completely laboratory research method that is not available for remote sensing.

Table 1 Summary of selected sensing performance of various schemes employed to detect nitrous oxide gases

Sensing scheme	Main target gas	Detection limit (measured)	Response time (seconds)	Temperature (°C)	Portability	Regeneration temperature (°C)	Reference
ChemFET and (Raman analysis)	NO_2	1–5 ppm (100 ppm)	61	150 (24)	Lab based	Yes at 150 °C	26
ChemFET	NO_2	2 ppm	<600	Room temperature	Lab based	Yes at 200 °C	60
Chemiresistor	NO_2	6 ppm	600	Room temperature	Lab based	Yes using UV	62
Chemiresistor	NO_2	5–10 ppb	600	165	Lab based	Yes at 330 °C	63
ChemFET/PEI	NO	200 ppb	70	Room temperature	Possible *in situ*	Yes, no detail	64
MOS	N_2O	10–300 ppm	10 (at 500 °C)	300–600	Possible *in situ*	Yes 500 °C	22
	N_2O	5–50 ppm	<60	Room temperature	Possible *in situ*	N.A	65
Fourier transform infrared (FT-IR) spectrometer							
FTIR detection	N_2O	5 ppb	600	Room temperature	Possible *in situ*	N.A	66
Chemical absorption optical fibre	N_2O (pure)	1 ppb	240	Room temperature	Possible *in situ*	—	67

Comparing this detection approach to the conventional spectroscopy techniques described in the introduction, these have good limits of detection, but are laboratory based and are not suitable for remote sensing applications. There are detection techniques that are being researched based upon optical fibre devices[23,66] such as a hollow waveguide design in conjunction with FTIR spectrometry yielding a detection limit of 5 ppb but again not suitable for remote fieldwork. Another design, using an end-coated optical fibre demonstrated a very low detection limit of 1 ppb, but provided no evidence of chemical selectivity or refractive index cross talk sensitivity.[67]

Conclusions

To the best of the authors' knowledge, this is the first report of SWNTs' optical properties, working with any other transducer material layer that has been used as a means to detect and monitor N_2O gas levels by an optical method; monitoring changes in effective refractive index and not an investigative spectroscopic analysis technique such as used in ref. 26. Importantly, such sensors have excellent regeneration and work at room temperature. The SWNT-LSP platform uses a very simple detection scheme, which can be made small and portable with the possibility of use in flammable and explosive environments. Moreover, the use of the optical properties of SWNT in conjunction with the functional polymer PEI demonstrated the selective detection of a nitrous oxide gas compared to other more common types of greenhouse gases; methane and carbon dioxide. In addition, the combination of CNTs with a functional polymer layers that enhances the specific spectral response to molecule species working together with this two-dimensional nanostructured plasmon sensing platform offers another paradigm that allows us to create sensors for simultaneous detection of multiple gases through the use of multiplexing or distributed fibre sensors.

Conflicts of interest

There are no conflicts to declare.

References

1 X. Jiang, Z. Cao, Y. Zhang, Z. Yuan, Z. Lou, X. Xu and X. Wang, *Chemosphere*, 2018, **195**, 351–364.
2 Z. A. AlOthman, Z. Abdullah and S. M. Wabaidur, *Arabian J. Chem.*, 2019, **12**(5), 633–651.
3 S. Seungju, I. Jeon, Y. Sato, C. Delacou, A. Anisimov, K. Suenaga, E. Kauppinen, Y. Matsuo and S. Maruyama, *APS March Meeting, Properties of Carbon Nanotubes*, Los Angeles, USA, 2018.
4 Z. Yi, Y. Bai and B. Yan, *Drug discovery today*, 2010, **15**(11), 428–435.
5 T. Zhang, S. Mubeen, N. V. Myung and M. A. Deshusses, *Nanotechnology*, 2008, **19**, 332001.
6 S. Chopra, K. McGuire, N. Gothard, A. M. Rao and A. Pham, *Appl. Phys. Lett.*, 2003, **83**(11), 2280–2282.
7 Y. Wang and J. TW Yeow, *J. Sens.*, 2009, **2009**, 493904.
8 L. Xiao, S. Cheng, H. Liu, S. Hu, D. Zhang and H. Ning, *Sensors*, 2012, **12**(7), 9635–9665.
9 P. Sumati, A. Maity, P. Banerji and S. B. Majumder, *Analyst*, 2014, **139**(7), 1796–1800.
10 G. Fine, L. M. Cavanagh, A. Afonja and R. Binions, *Sensors*, 2010, **10**(6), 5469–5502.
11 L. Yanfang, L. Chang, Y. Zhao, X. Meng, Y. Wei, X. Wang, J. Yue and T. Liu, *Measurement*, 2016, **79**, 211–215.
12 IPCC Intergovernmental Panel on Climate Change (IPCC), *Climate Change 2013: The Physical Science Basis*, Cambridge University Press, N. Y, USA, 2013.
13 S. Solomon, in *IPCC (2007) Climate Change 2007: The Physical Science Basis. Contribution of Working Group I to the Fourth Assessment Report of the Intergovernmental Panel on Climate Change*, Cambridge Univ Press, Cambridge, UK, 2007.
14 A. R. Ravishankara, J. S. Daniel and R. W. Portmann, *Science*, 2009, **326**, 5949.
15 O. A. Zaw, S. Sudo, K. Inubushi, M. Mano, A. Yamamoto, K. Ono and T. Osawa, *Agric., Ecosyst. Environ.*, 2018, **252**, 148–158.
16 M. J. Eichner, *J. Environ. Qual.*, 1990, **19**(2), 72–280.
17 K. H. Becker, J. C. Lörzer, R. Kurtenbach, P. Wiesen, T. E. Jensen and T. J. Wallington, *Environ. Sci. Technol.*, 1999, **33**(22), 4134–4139.

18 W. G. Zumft and P. M. H. Kroneck, *Adv. Microb. Physiol.*, 2006, **52**, 107–227.

19 E. A. Davidson, K. V. L. V. Savage, L. V. Verchot and R. Navarro, *Agric. For. Meteorol.*, 2002, **113**(1), 21–37.

20 C. Lammirato, U. Lebender, J. Tierling and J. Lammel, *J. Plant Nutr. Soil Sci.*, 2018, **181**(1), 78–89.

21 I. Yuzuru, Y. T. Gao, S. P. Panda, L. J. Roman, B. S. S. Masters and S. T. Weintraub, *Biochem. Biophys. Res. Commun.*, 2005, **338**(1), 543–549.

22 K. Eiichi, G. Sakai, K. Shimanoe, Y. Kanmura, Y. Teraoka, N. Miura and N. Yamazoe, *Sens. Actuators, B*, 2001, **77**(1), 72–77.

23 T. D. Rapson and H. Dacres, *TrAC, Trends Anal. Chem.*, 2014, **54**, 65–74.

24 K. Andersen, T. Kjær and N. P. Revsbech, *Sens. Actuators, B*, 2001, **81**(1), 42–48.

25 D. D. Nelson, B. McManus, S. Urbanski, S. Herndon and M. S. Zahniser, *Spectrochim. Acta*, 2004, **60**(14), 3325–3335.

26 D. V. Ponnuvelu, J. Dhakshinamoorthy, A. K. Prasad, S. Dhara, M. Kamruddin and B. Pullithadathil, *ACS Appl. Nano Mater.*, 2020, **3**, 5898–5909.

27 T. Allsop, R. Neal, E. M. Davies, C. Mou, P. Brown, S. Rehman, K. Kalli, D. J. Webb, P. Calverhouse and I. Bennion, *Meas. Sci. Technol.*, 2010, **21**(9), 4029.

28 E. D. Palik, *Handbook of Optical Constants of Solids*, Academic, New York, 1998.

29 T. Allsop, R. Neal, C. Mou, P. Brown, S. Rehman, K. Kalli, D. J. Webb, D. Mapps and I. Bennion, *Opt. Fiber Technol.*, 2009, **15**(5), 477–482.

30 T. Allsop, R. Neal, M. Dvorak, K. Kalli, A. Rozhin and D. J. Webb, *Opt. Express*, 2013, **21**(16), 18765–18776.

31 T. Allsop, R. Neal, C. Mou, S. Saied, S. Rehman, K. Kalli, K. D. J. Webb, P. F. Culverhouse, J. D. Sullivan, D. Mapps and I. Bennion, *IEEE J. Quantum Electron.*, 2012, **48**(3), 394–405.

32 https://www.cargille.com/refractive-index-liquids/.

33 A. M. Bronstein and R. Kimmel, *Numerical Geometry of Non-rigid Shapes*, Springer Science & Business Media, Berlin, 2008.

34 M. Shim, A. Javey, N. W. Shi Kam and H. Dai, *J. Am. Chem. Soc.*, 2001, **123**(46), 11512–11513.

35 A. Star, J.-C. P. Gabriel, K. Bradley and G. Grüner, *Nano Lett.*, 2003, **3**(4), 459–463.

36 V. B. Neustruev, *J. Phys.: Condens. Matter*, 1994, **6**(35), 6901.

37 T. Allsop, R. Neal, V. Kundrat, C. Wang, C. Mou, P. Culverhouse, J. D. Ania-Castanon, K. Kalli and D. J. Webb, *Opt. Lett.*, 2019, **44**, 195–198.

38 P. Cordier, J. C. Doukhan, E. Fertein, P. Bernage, P. Niay, J. F. Bayon and T. Georges, *Opt. Commun.*, 1994, **111**(3–4), 269–275.

39 J. Ado, E. Kauppinen and A. Hassanien, Carbon-nanotube metrology, in *Carbon Nanotubes*, Springer, Berlin, Germany, 2007.

40 H. Kataura, Y. Kumazawa, Y. Maniwa, I. Umezu, S. Suzuki and Y. Ohtsuka, *Synth. Met.*, 1999, **103**, 2555–2558.

41 M. Milnera, J. Kurti, M. Hulman and H. Kuzmany, *Phys. Rev. Lett.*, 2000, **84**, 1324–1327.

42 J. Homola and M. Piliarik, Surface plasmon resonance (SPR) sensors, in *Surface Plasmon Resonance Based Sensors*, Springer, Berlin, Germany, 2006, pp. 45–67.

43 K. K. Lance, E. Coronado, L. Zhao and G. C. Schatz, *The optical properties of metal nanoparticles: the influence of size, shape, and dielectric environment*, ACS Publications, 2003, vol. 107, pp. 668–677.

44 N. Supawadee, P. Khongpracha, Y. Tantirungrotechai and J. Limtrakul, *J. Mol. Graphics Modell.*, 2007, **26**(1), 179–186.

45 N. Shinichi, M. Yudasaka, K. Hirahara and T. Ichihashi, *Chem. Phys. Lett.*, 2000, **328**(4), 374–380.

46 T. Allsop, V. Kundrat, K. Kalli, G. B. Lee, R. Neal, P. Bond, B. Shi, J. Sullivan, P. Culverhouse and D. J. Webb, *Sens. Actuators, B*, 2018, **255**(1), 843–853.

47 T. Allsop, R. Arif, R. Neal, K. Kalli, V. Kundrát, A. Rozhin, P. Culverhouse and D. J. Webb, *Light: Sci. Appl.*, 2016, **5**, e16036.

48 J. Hu, X. Sun, A. Agarwal and L. C. Kimerling, *J. Opt. Soc. Am. B*, 2009, **26**, 1032–1041.

49 M. M. Andersson and R. Hatti-Kaul, *J. Biotechnol.*, 1999, **72**(1), 21–31.

50 V. A. Markel, *J. Opt. Soc. Am. A*, 2016, **33**, 71244–71256.

51 N. Hedin, L. Chen and A. Laaksonen, *Nanoscale*, 2010, **2**(10), 1819–1841.

52 Y. Chu, D. Tang, Z. Ke, J. Ma and R. Li, *J. Appl. Polym. Sci.*, 2017, **134**(16).

53 N. Mehio, S. Dai and D. Jiang, *J. Phys. Chem. A*, 2014, **118**(6), 1150–1154.

54 Y. Cui, H. Kita and K.-i. Okamoto, Preparation and gas separation properties of zeolite T membrane, *Chem. Commun.*, 2003, **17**, 2154–2155.

55 T. Matsufuji, N. Norikazu, K. Ueyama and M. Matsukata, *Catal. Today*, 2000, **56**(1), 265–273.

56 G. A. Niklasson, C. G. Granqvist and O. Hunderi, *Appl. Opt.*, 1981, **20**(1), 26–30.

57 P. Qi, O. Vermesh, M. Grecu, A. Javey, Q. Wang, H. Dai, S. Peng and K. J. Cho, *Nano Lett.*, 2003, **3**(3), 347–351.

58 B. Kumanek and D. Janas, *J. Mater. Sci.*, 2019, **54**(10), 7397–7427.

59 W. Bao, F. Miao, Z. Chen, H. Zhang, W. Jang, C. Dames and C. N. Lau, *Nat. Nanotechnol.*, 2009, **4**(9), 562.

60 J. Kong, N. R. Franklin, C. Zhou, M. G. Chapline, S. Peng, K. Cho and H. Dai, *Science*, 2000, **287**(5453), 622–625.

61 http://www.goodfellow.com/E/Polyetherimide.html.

62 J. Li, Y. Lu, Q. Ye, M. Cinke, J. Han and M. Meyyappan, *Nano Lett.*, 2003, **3**(7), 929–933.

63 L. Valentini, F. Mercuri, I. Armentano, C. Cantalini, S. Picozzi, L. Lozzi, S. Santucci, A. Sgamellotti and J. M. Kenny, *Chem. Phys. Lett.*, 2004, **387**, 356–361.

64 O. Kuzmych, B. L. Allen and A. Star, *Nanotechnology*, 2007, **18**(37), 375502.

65 J. F. Petruci, E. Tütüncü, A. A. Cardoso and B. Mizaikoff, *Appl. Spectrosc.*, 2019, **73**(1), 98–103.

66 J. F. Petruci, A. Wilk, A. A. Cardoso and B. Mizaikoff, *Sci. Rep.*, 2018, **8**(1), 5909.

67 S. I. B. Lurdes, T. A. P. Rocha-Santos and A. C. Duarte, *J. Environ. Monit.*, 2009, **11**(4), 852–857.